Hildén, Panu; Kaivola, Matti; Shevchenko, Andriy

Prism-based approach to create intensity-interferometric non-diffractive cw light sheets

Published in:
Optics Express

DOI:
10.1364/OE.458719

Published: 04/07/2022

Document Version
Publisher's PDF, also known as Version of record

Research Article | Vol. 30, No. 14 / 4 Jul 2022 / Optics Express 24716

Optics EXPRESS

Prism-based approach to create intensity-interferometric non-diffractive cw light sheets

PANU HILDÉN,* MATTI KAIVOLA, AND ANDRIY SHEVCHENKO

Department of Applied Physics, Aalto University, P.O. Box 13500, FI-00076 Aalto, Finland
*panu.hilden@aalto.fi

Abstract: Light sheets are optical beam-like fields with one-dimensional intensity localization. Ideally, the field intensity should be independent of the longitudinal and one of the transverse coordinates, which is difficult to achieve even for truncated light sheets. In this work, we present a general theoretical framework for intensity-interferometric continuous wave (cw) light sheets formed by overlapping the interference fringe patterns of mutually uncorrelated frequency components of the field. We show that the key parameters of the light sheets can be calculated using simple analytical expressions. We propose a practical way to generate such light sheets with the help of prisms and demonstrate numerically the abilities of the method. Both bright and dark light sheets with an exceptionally small thickness and long divergence-free propagation distance are possible to generate. We also show that the transverse profile of the generated light sheets can be shaped by modifying the spectrum of the light. We believe our findings advance the beam-engineering technology and its applications.

1. Introduction

Light sheet is an optical beam, the intensity of which is strongly localized along one transverse direction, as in a beam of light focused with a cylindrical lens. Applications of light sheets are found in wireless optical communication [1,2], optical tweezers [3,4], plasmonics [5,6], spectroscopy [7,8], and microscopy [9–11]. For these applications, light sheets with a narrow width maintained over a long propagation distance, possibly also in the presence of turbulence and scattering, are desired. Ideally, a light sheet should be diffraction-free and self-healing, similarly to a Bessel beam [12,13], but with the intensity localized only in one dimension. Examples of such 1D-localized optical fields are Airy beams, the intensity peaks of which move along a parabolic trajectory [14,15], and interference fringe patterns formed by two mutually coherent plane waves that propagate in different directions. The interference pattern of two plane waves with the transverse wave numbers $\pm k_x$ is given by a cosine function $\cos k_x x$, which is why such a beam is often called a cosine beam [16]. However, calling an interference fringe pattern an optical beam is a bit misleading, as it contains an infinite energy equally distributed between an infinite number of identical intensity peaks along the transverse direction. In practice, plane waves are replaced by collimated optical beams, which makes the number of transverse intensity maxima and the diffraction-free propagation length finite. The beams are usually derived from a single beam by splitting it with an isosceles prism, a diffraction grating, or an opaque screen with two parallel slits followed by a cylindrical lens [16,17].

In an effort to generate a diffraction-free light sheet with a single, strong, and narrow intensity peak and significantly reduced sidelobes in the transverse profile, many approaches have been proposed. While apodization can be used to essentially eliminate the sidelobes [17], the resulting light sheet will have a relatively short propagation distance. An alternative approach is to prevent the perfect constructive interference away from the beam axis. For this purpose, masks with binary phase and amplitude profiles have been developed [18–21]. A light sheet produced

#458719 https://doi.org/10.1364/OE.458719
Journal © 2022 Received 17 Mar 2022; revised 6 Jun 2022; accepted 7 Jun 2022; published 24 Jun 2022

Optics EXPRESS

by using such a mask placed in front of a cylindrical lens has small sidelobes, but is slowly diverging. For a strictly non-diverging light sheet, the interference of broadband optical beams can be utilized. The frequency components of the beams form standing wave patterns with varying transverse wave numbers $k_x(\omega)$, and the interference of all these components is perfectly constructive only at the beam axis, resulting in a higher intensity of the central peak. Pulsed light sheets created by using this approach, referred to as space-time wave packets, have attracted much of attention in the scientific community (see, e.g., Ref. [22] and references therein). The approach has also been used to generate dark sheets, where the central peak is replaced by an intensity dip. Since in pulsed light, the frequency components correlate, light sheets are localized also in the longitudinal direction. If, on the other hand, the frequency components are mutually incoherent, a cw counterpart of such a space-time wave packet can be generated [23]. Incoherent light has also been used to generate light sheets based on the field synthesis method introduced in Ref. [24]. The field synthesis method uses a focused light line scanned over an annular mask on the back focal plane of a microscope objective, creating a continuum of cosine-shaped intensity patterns with varying spatial frequencies [24,25]. Instead of scanning, the field synthesis can be static, if the mask is illuminated by mutually incoherent light lines simultaneously, which has also been realized using both spatially and temporally incoherent light [26,27].

In this work, we consider light sheets in the form of a superposition of interference-fringe patterns of mutually incoherent frequency components of the optical field used. The intensity distribution due to the *intensity interference*[28–30] of the frequency components is investigated analytically. For a light sheet with a Gaussian spectrum, we show how the suppression of the sidelobes and the width of the light sheet depend on the spatial-frequency bandwidth and the transverse wavenumber of the central frequency component. A large spatial-frequency bandwidth and a high positive angular dispersion would be needed to obtain a thin light sheet with suppressed sidelobes. Then we introduce a compact prism-based system for generation of such light sheets. The angular dispersion is enhanced by using a compound prism design, similar to the one proposed in Ref. [31]. The performance of the system is studied by using numerical examples. We also show that the properties of the generated light sheets can be considerably improved by shaping the spectrum of the light used. We expect our findings to advance the development of light sheets for a variety of optical applications.

The paper is organized as follows. Section 2 introduces a theoretical basis for non-diffractive cw light sheets. In Section 3, a prism-based optical system for light-sheet generation is proposed and analyzed. Section 4 presents a way to improve the properties of the generated light sheets by shaping the spectrum of the incident light. Conclusions are drawn in Section 5.

2. Intensity-interferometry-based cw diffraction-free light sheets

The intensity distribution of a light sheet represents the intensity interference of its frequency components, if the components are mutually incoherent. In other words, the interference fringes produced by the pairs of equal-frequency components overlap and form a cw light sheet. The total intensity distribution can be calculated as

$$I(x) = \int_0^\infty S(\omega)\cos^2[k_x(\omega)x]d\omega, \tag{1}$$

where $S(\omega)$ is the power spectral density of the light. We assume that the light sheet lies in the yz-plane. The transverse wave number can be written in terms of the propagation angle α as $k_x(\omega) = \omega/c \sin\alpha(\omega)$; note that, in general, $\alpha(\omega)$ is a function of frequency determined by the used beam converter, optical element producing the two interfering beams out of the original collimated beam. Let the original beam have a Gaussian spectrum $S(\omega) = E_0^2/\Delta\omega \exp[-2(\frac{\omega-\omega_0}{\Delta\omega})^2]$ with the center frequency ω_0, amplitude E_0, and spectral bandwidth $\Delta\omega$. Note that we define the spectral density such that the intensity is given by $|E|^2$, to shorten the notation. We can assume that, within the field bandwidth, angle $\alpha(\omega)$ is linear, so that $\sin\alpha(\omega)$ can be expanded as

$$\sin\alpha(\omega) = \sin\alpha_0 + \cos\alpha_0\partial_\omega\alpha_0(\omega-\omega_0), \tag{2}$$

where α_0 and $\partial_\omega\alpha_0$ are the propagation angle and its derivative with respect to ω at the center-frequency ω_0, respectively. The second quantity is called the angular dispersion. With this expansion, the integral in Eq. (1) can be solved analytically. The exact expression, found in appendix A, is lengthy, but close to the axis of the light sheet, it can be reduced to

$$I(x) = E_0^2\sqrt{\frac{\pi}{8}}\left\{1+\exp\left[-\frac{1}{2}(\Delta k_x x)^2\right]\cos[2k_x(\omega_0)x]\right\}, \tag{3}$$

where Δk_x is the bandwidth of the spatial-frequency spectrum given approximately by

$$\Delta k_x = \frac{\Delta\omega(\cos\alpha_0\partial_\omega\alpha_0\omega_0+\sin\alpha_0)}{c}. \tag{4}$$

The intensity distribution described by Eq. (3) resembles that of the center-frequency component $|E_0\cos[k_x(\omega_0)x]|^2$ truncated by a Gaussian envelope centered at $x=0$ (see Fig. 1(a)). The width of the envelope is inversely proportional to Δk_x, as expected.

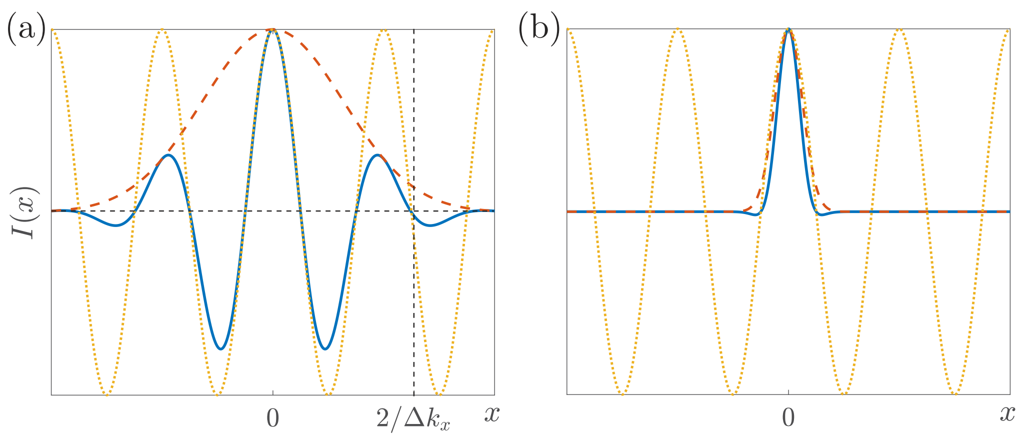

Fig. 1. Transverse intensity distributions of light sheets with spatial-frequency bandwidth (a) $\Delta k_x = k_x(\omega_0)/2$ and (b) $\Delta k_x = 8k_x(\omega_0)/\pi$. The yellow dotted curve shows the intensity distribution of the central frequency component that, when truncated by the envelope corresponding to the orange dashed line, yields the light sheet intensity introduced by the blue solid line.

For a sufficiently large bandwidth, $\Delta k_x > 8k_x(\omega_0)/\pi$, the envelope is narrower than the central intensity peak, and all the sidelobes are eliminated, yielding a light sheet with a single intensity peak (see Fig. 1(b)). The intensity distribution can then be approximated with the help of the Taylor series expansion as

$$\exp\left[-\frac{1}{2}(\Delta k_x x)^2\right]\cos[2k_x(\omega_0)x] = 1-\left(2k_x(\omega_0)^2+\frac{\Delta k_x^2}{2}\right)x^2. \tag{5}$$

In this case, the full width at half maximum (FWHM) of the light sheet intensity distribution is found to be

$$W = \frac{2}{\sqrt{4k_x(\omega_0)^2+\Delta k_x^2}}, \tag{6}$$

where the half maximum refers to the midpoint between the peak intensity $\sqrt{\pi/2}E_0^2$ and the constant background intensity $\sqrt{\pi/8}E_0^2$.

Optics EXPRESS

So far, it has been assumed that the plane waves of each frequency component are in phase at $x = 0$. However, in general, they can have some phase difference φ, in which case the standing wave pattern for each particular pair of plane waves is determined by

$$E(x) = \frac{E_0}{2}[\exp(ik_x x) + \exp(i\varphi)\exp(-ik_x x)] = E_0 \cos\left(k_x x - \frac{\varphi}{2}\right)\exp\left(\frac{i\varphi}{2}\right). \tag{7}$$

The phase difference can be introduced with a phase mask placed between the light source and the beam converter. In case of a fixed phase difference for all frequency components, Eq. (3) is generalized to take the form

$$I(x) = E_0^2\sqrt{\frac{\pi}{8}}\left\{1 + \exp\left[-\frac{1}{2}(\Delta k_x x)^2\right]\cos[2k_x(\omega_0)x - \varphi]\right\}, \tag{8}$$

as shown in appendix A. If the phase difference is equal to π, a dark sheet is produced instead of a bright one. The intensity distribution is then given by

$$I(x) = E_0^2\sqrt{\frac{\pi}{8}}\left\{1 - \exp\left[-\frac{1}{2}(\Delta k_x x)^2\right]\cos[2k_x(\omega_0)x]\right\}. \tag{9}$$

The dark sheet has a zero intensity at the beam axis surrounded by a non-zero background intensity.

We analyzed the experimentally obtained light sheets of Ref. [23] by using our equations. In the experiments of Ref. [23], the angular dispersion (spatio-temporal correlation) is introduced by using a $4f$-type optical system. The frequency components are separated spatially by a diffraction grating followed by a lens and they are phase-modulated using a spatial light modulator (SLM). The phase modulation profile of the SLM is orthogonal to the spectral separation direction. The SLM splits each frequency component into two waves with prescribed spatial frequencies $\pm k_x$. The separated frequency components are then recombined using another lens followed by a diffraction grating. In Ref. [23], phase differences $\varphi = \pi/2$ and $\varphi = \pi$ were experimentally realized by covering half of the SLM with a glass slide. The results seem to agree with the generalized intensity distribution given by Eq. (8). The ingenious setup for space-time light sheet generation, described in more detail in Refs. [22,23,32,33], allows one to control the angular dispersion and the group velocity of pulsed light sheets in free space [22,32,34]. The system is rather universal, but it is large and such that obtaining thin light sheets is problematic. In the next section, we introduce a very simple and compact optical system that is able to generate also exceptionally thin cw light sheets.

3. Generation of light sheets using prisms

In the previous section, we have found that, for creating a thin light sheet with reduced sidelobes, a broad spatial-frequency bandwidth Δk_x is required. According to Eq. (4), this can be obtained by utilizing an optical element with a large positive angular dispersion $\partial_\omega \alpha$, for example, a prism.

Figure 2 illustrates a wide collimated beam of light refracted by an isosceles prism. The finite size of the prism base $2R$ apodizes the beam and makes the wave interference region finite. The propagation of the apodized and refracted beam can be studied by applying the Fresnel-Kirchhoff

Optics EXPRESS

diffraction integral to each frequency component. The intensity of the total field is then given by

$$
\begin{aligned}
I(x,z) = &\int_0^\infty S(\omega)\Bigg|\sqrt{\frac{k}{2\pi z}}\exp\left[i\left(kz-\frac{\pi}{4}\right)\right]\\
&\times\int_{-R}^{R}[\exp(ik_x x')+\exp(i\varphi)\exp(-ik_x x')]\exp\left[i\frac{k}{2z}(x-x')^2\right]dx'\Bigg|^2 d\omega\\
&=\frac{E_0^2}{16\Delta\omega}\int_0^\infty \exp\left[-2\left(\frac{\omega-\omega_0}{\Delta\omega}\right)^2\right]\\
&\times\Bigg|\exp(ik_x x)\left(\operatorname{erf}\left\{\frac{(1-i)[k(R+x)-k_x z]}{\sqrt{2kz}}\right\}+\operatorname{erf}\left\{\frac{(1-i)[k(R-x)+k_x z]}{\sqrt{2kz}}\right\}\right)\\
&+\exp(i\varphi)\exp(-ik_x x)\left(\operatorname{erf}\left\{\frac{(1-i)[k(R+x)+k_x z]}{\sqrt{2kz}}\right\}+\operatorname{erf}\left\{\frac{(1-i)[k(R-x)-k_x z]}{\sqrt{2kz}}\right\}\right)\Bigg|^2 d\omega,
\end{aligned}
\tag{10}
$$

where φ takes the value of 0 or π for the cases of light and dark sheets, respectively. The apodization limits the diffraction-free propagation distance to $z_{\max} = R/\tan(\alpha) - R/\tan(\gamma/2)$, as illustrated in Fig. 2. Using the method of stationary phase applied to the light sheet at the beam axis [17], one can find that Eq. (10) is reduced to Eqs. (3) and (9) for the light and dark sheets, respectively.

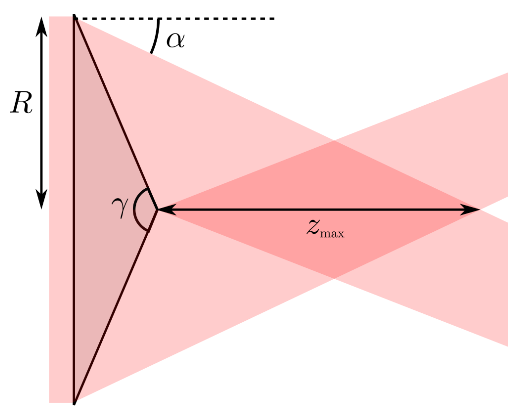

Fig. 2. A collimated optical beam refracted by an isosceles prism. The resulting standing-wave pattern is formed within the distance $z_{\max}$ behind the apex of the prism.

The angular dispersion introduced by the prism can be high, if the light is incident on the refracting surface of the prism at an angle close to the critical angle of total internal reflection (TIR), which is used in the angular-dispersion amplifiers [35,36]. Indeed, the refraction angle $\theta_2(\omega)$ is given by Snell's law

$$\theta_2(\omega) = \arcsin\frac{n_1(\omega)\sin\theta_1}{n_2(\omega)}, \tag{11}$$

which leads to the expression

$$\partial_\omega\theta_2 = \frac{(\partial_\omega n_1 - \frac{n_1}{n_2}\partial_\omega n_2)\sin\theta_1}{\sqrt{n_2^2 - n_1^2\sin^2\theta_1}}. \tag{12}$$

Here, n_1 and n_2 are the refractive indices of the media inside and outside the prism. Equation (12) shows that at the critical angle of TIR, the angular dispersion $\partial_\omega\theta_2$ approaches infinity. Therefore,

Optics EXPRESS

using a prism with a small apex angle γ would result in a thin light sheet with reduced sidelobes. Unfortunately, this method is problematic for the following two reasons: (1) the reflection losses near TIR are large and highly depended on the frequency and (2) the propagation direction of the refracted light is almost parallel to the prism surface, making the diffraction-free propagation distance $z_{\max}$ very short. In the following, we propose to solve both of these problems by using a compound prism, where two additional prisms are placed next to the original one (see Fig. 3). Refraction of light at the boundary between the primary prism (with refractive index n_1 and apex angle γ_1) and the secondary prisms (with parameters n_2 and γ_2) introduces the following angular dispersion

$$\partial_\omega \beta = \frac{(\partial_\omega n_1 - \frac{n_1}{n_2}\partial_\omega n_2)\cos\frac{\gamma_1}{2}}{\sqrt{n_2^2 - n_1^2\cos^2\frac{\gamma_1}{2}}}. \tag{13}$$

To be able to maximize this quantity near the critical angle of TIR, we select $n_1 > n_2$ and $\cos\gamma_1/2$ close to n_2/n_1. Additionally, we look for the prism materials with large and small material dispersion for the primary and secondary prisms, respectively ($\partial_\omega n_1 \gg \partial_\omega n_2$). Finally, the index difference $\Delta n = n_1 - n_2$ should be small, which not only increases the angular dispersion, but also minimizes the losses due to the reflection at the boundaries between the prisms.

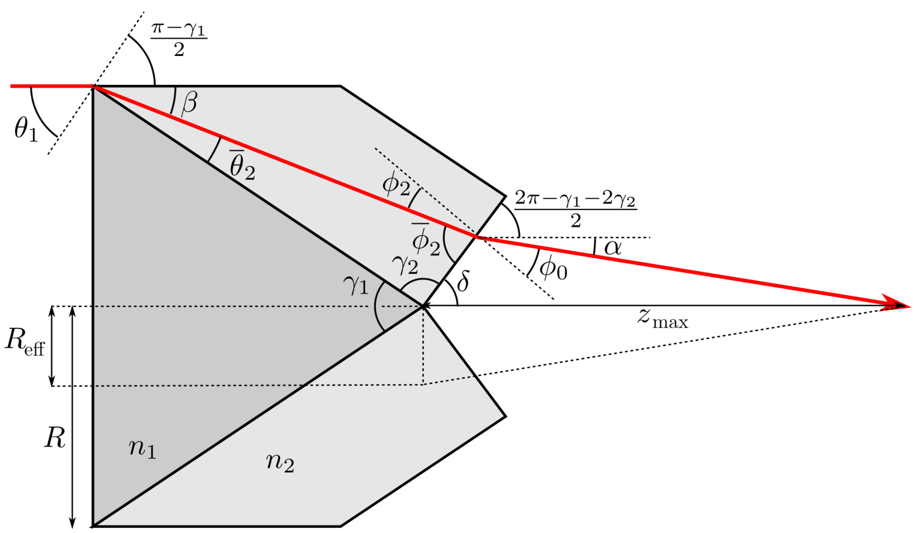

Fig. 3. A peripheral ray (red arrow) transmitted trough a compound prism. The refractive indices of the primary and secondary prisms are n_1 and n_2, respectively. The prisms are surrounded by free space.

In addition to reducing reflection losses, the secondary prisms introduce additional refraction, thereby extending the diffraction-free propagation distance $z_{\max}$, as shown in Fig. 3. For small angles α, the diffraction-free propagation distance $z_{\max}$ is given by the following approximate expression

$$z_{\max}(\omega) = \frac{\tan\overline{\theta}_2(\omega)}{\tan\alpha(\omega)}R. \tag{14}$$

The above equation shows that, in order to counteract the reduction of $z_{\max}$, the angle α should satisfy the inequality $\alpha < \overline{\theta}_2$. Alongside the reduced reflection losses, this condition limits the operation of the compound prism not to take place too close to TIR at the refraction between the prisms.

An additional remarkable property of the setup is that the secondary prisms can enhance the angular dispersion introduced by the first refraction. Using the fact that the propagation angle α is given by (see Fig. 3)

$$\alpha = \frac{\pi}{2} - \delta + \arcsin\left[\frac{n_2}{n_0}\cos(\beta - \frac{\gamma_1}{2} - \gamma_2)\right], \tag{15}$$

the angular dispersion of the compound prism as a whole is found to be

$$\partial_\omega \alpha = \frac{\cos(\phi_2) n_2 \partial_\omega \beta - \sin(\phi_2)\partial_\omega n_2}{\sqrt{n_0^2 - n_2^2 \sin^2(\phi_2)}}. \tag{16}$$

It can be seen that, for a small angle ϕ_2, the second refraction amplifies the angular dispersion by a factor approximately equal to n_2.

As an application example of the above proposal, we designed a compound prism for light with a Gaussian frequency spectrum that has the central wavelength of $\lambda_0 = 440$ nm and FWHM of 10 nm. We choose zinc sulfide (ZnS) and LASF35-glass as the materials for the primary and secondary prisms, respectively. In this case, we obtain $n_1(\lambda_0) \approx 2.48$, $\partial_\lambda n_1(\lambda_0) \approx -1.4$ μm^{-1} [37], $n_2(\lambda_0) \approx 2.07$, and $\partial_\lambda n_2(\lambda_0) \approx -0.5$ μm^{-1} [38]. For the given materials, the apex angle γ_1 is selected for a near-TIR operation to be $\gamma_1 = 68.5°$. Finally, we choose the apex angle γ_2 of 103° to refract light at the longest wavelength of 450 nm along the beam axis.

For the designed ZnS-LASF35 prism, the propagation angles β and α as functions of the wavelength $\lambda \in [430\text{ nm}, 450\text{ nm}]$ are shown in Fig. 4(a). The edges of the design bandwidth are shown by the vertical dashed lines. The angular dispersion $\partial_\omega \beta$ is seen to be significantly amplified by the second refraction, yielding $\partial_\lambda \alpha_0 \approx -0.4°/\text{nm}$. Figure 4(b) shows the diffraction-free propagation distance $z_{\max}$ as a function of the wavelength. The distance $z_{\max}$ is at the central wavelength as long as $2R$. We note that, for a single ZnS prism (as in Fig. 2), the angular dispersion would be approximately 10 times smaller for comparable values of $z_{\max}$. The reflection losses can be seen in Figs. 4(c) and (d), where the transmittances for the air-ZnS (T_{01}), ZnS-LASF35 (T_{12}), and LASF35-air (T_{20}) boundaries are shown for both transverse electric (TE) and transverse magnetic (TM) polarizations of the transmitted light. The curves show that, despite operating near TIR, a significant portion of the incident light (about 30 % in total for the TE and about 50 % for the TM polarization) is transmitted by the compound prism. The reflected light exits the prisms at large angles and does not overlap with the light-sheet region. The reflection loss can be significantly reduced or eliminated also with the help of antireflection coatings.

Let us next use Eq. (10) to calculate the intensity distribution for a light sheet generated using the designed compound prism. We neglect the reflection losses and assume that $R = 10$ mm. The propagation angles are calculated from Eq. (15). The obtained intensity distribution is shown in Fig. 5(a); note the different scales for the vertical and horizontal axes. The thickness of the obtained light sheet is on the order of 1 μm only, and it stays essentially unchanged for a 15-mm propagation distance, i.e., 10^4 times longer than the thickness. The transverse profile (along the x-axis) of the light sheet at $z = 1$ μm is shown in Fig. 5(b). The blue curve results from Eq. (10), while the orange curve is obtained from the approximate Eq. (3). This shows that the dependence of α on ω in the relevant spectral range is close to linear and Eqs. (2) and (3) are quite accurate. Figure 5(c) illustrates the FWHM of the light sheet intensity distribution as a function of propagation distance z. It can be seen that for $z > 15$ mm, the width of the light sheet increases approximately linearly due to the far-field diffraction. It is interesting to note that the obtained diffraction-free propagation distance is over 2000 times longer than the equivalent distance calculated for a conventional light sheet with the same thickness; conventional light sheets are obtained by focusing a laser beam with a cylindrical lens or with a spherical lens when

Optics EXPRESS

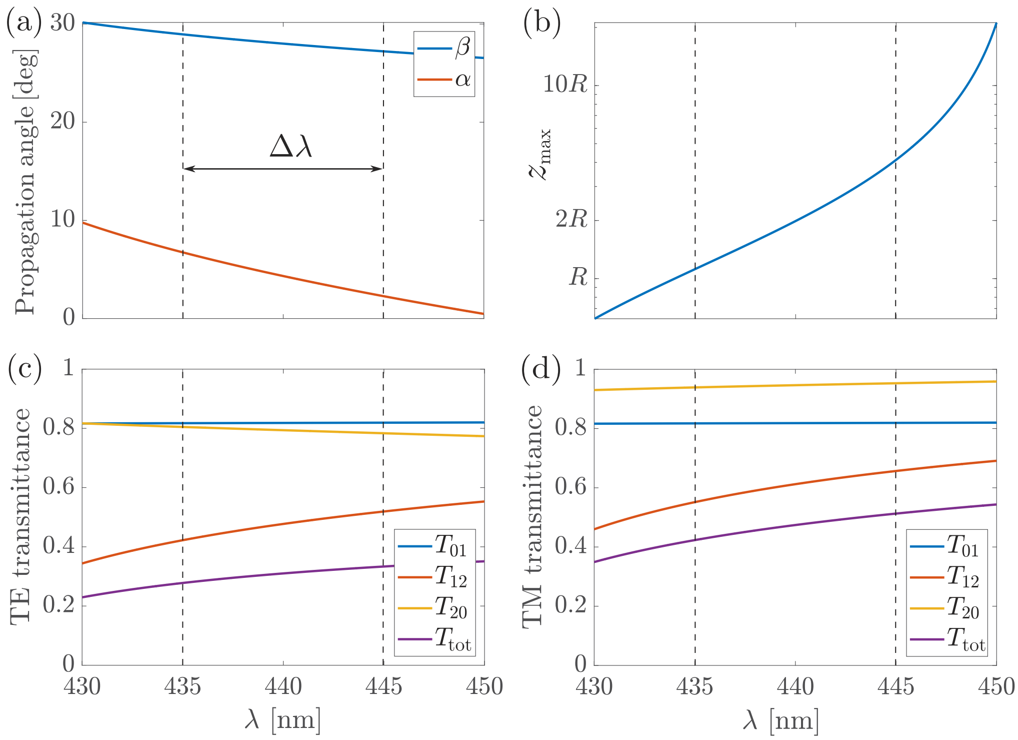

Fig. 4. Spectral properties of the designed ZnS-LASF35 compound prism: (a) propagation angles β in LASF35 prism and α in free space, (b) diffraction-free propagation distance $z_{\max}$ in a logarithmic scale, and (c),(d) the values of transmittance of TE/TM-polarized waves at the boundaries between air and ZnS (T_{01}), ZnS and LASF35 (T_{12}), LASF35 and air (T_{20}), as well as the total transmittance T_{tot}.

applying beam scanning. If necessary, the off-axis background light can be attenuated by an aperture, which will lead to an increase of the divergence of the light sheet. Hence, depending on the application, a compromise between the low background intensity and low-divergence propagation length can be found. We also note that the approach can be applied to create pulsed light sheets, for which the incident cw beam is simply replaced with a pulsed beam. Similar characteristics are expected to be obtained as for cw sheets as long as the pulses at the output of the prisms are not considerably chirped.

To generate a dark sheet instead of a bright one, a half of the front surface of the primary prism is covered with a dielectric film that shifts the phase of the incident light by π. Figure 6(a) shows the transverse intensity distribution obtained for this case by using Eqs. (9) and (10). The profile shows a zero intensity at the beam-axis surrounded by two intensity peaks and a constant background intensity environment. Again, an approximate analytical expression in Eq. (9) gives a rather accurate profile. The intensity distribution of the dark sheet in the xz-plane is shown in Fig. 6(b), from which the diffraction-free propagation distance is seen to be equal to that of the bright counterpart considered above.

Optics EXPRESS

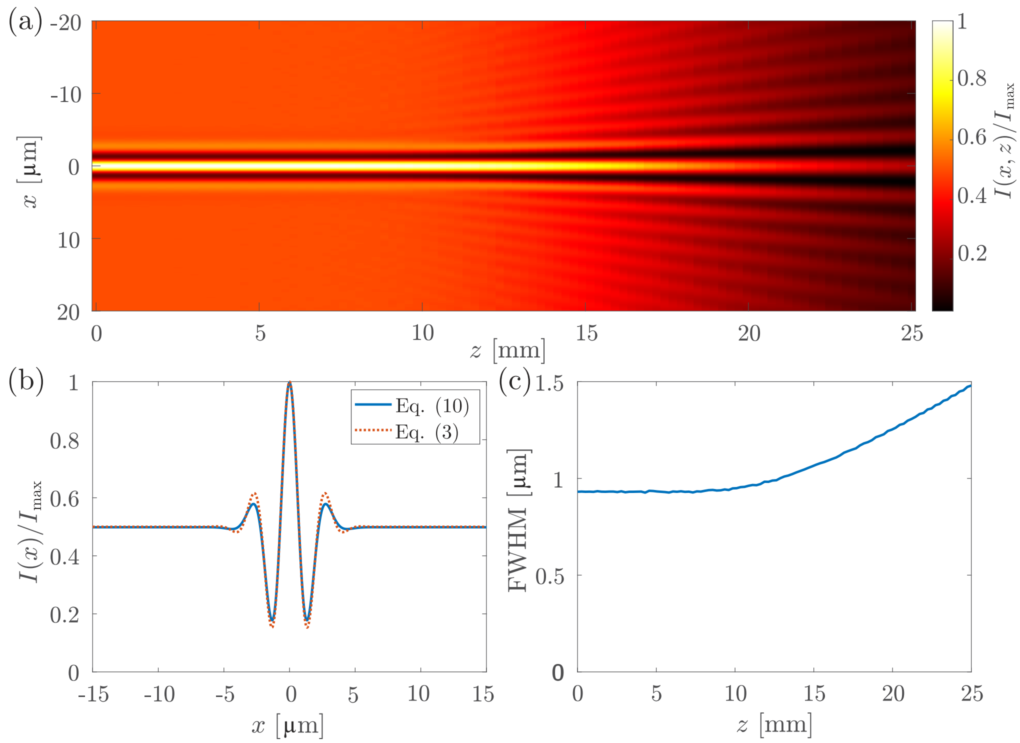

Fig. 5. Properties of a light sheet generated by using the designed compound prism: (a) the intensity distribution in the *xz*-plane; (b) the transverse intensity profile along the *x*-axis at $z = 1$ μm (here the blue and orange dotted lines are obtained from Eqs. (10) and (3), respectively); (c) the FWHM of the light sheet as a function of propagation distance *z*.

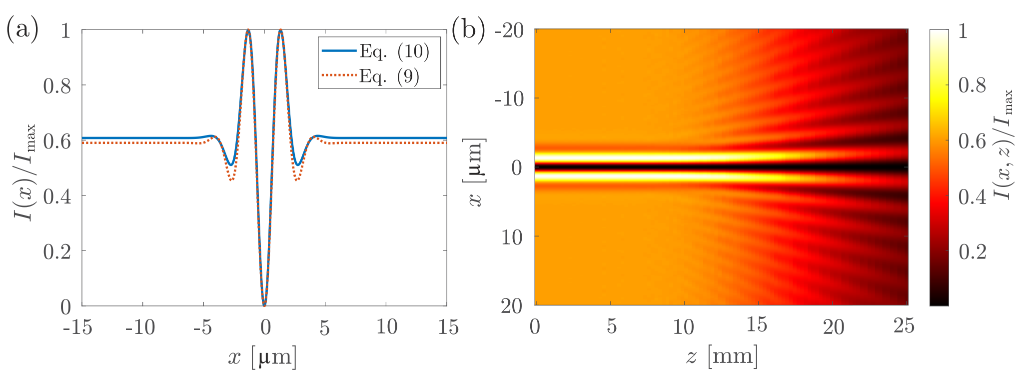

Fig. 6. Properties of a dark sheet generated by using the designed compound prism: (a) the transverse intensity profile along the *x*-axis at $z = 1$ μm (here the blue and orange dotted lines are obtained from Eqs. (10) and (9), respectively); (b) the intensity distribution in the *xz*-plane.

Optics EXPRESS

4. Shaping the light-sheet profile by changing the spectrum

Light sheets obtained in the above section exhibit a noticeable spatial oscillation of the intensity around the central maximum. The same feature has been observed also in the experiments of Ref. [23]. For some applications, however, such extra oscillations can be unwanted (e.g., for applications in light sheet microscopy). In this section, we propose a method to suppress the extra oscillations by modifying the spectrum of the incident light.

The problem with use of Gaussian spectra is that the frequency components close to the central frequency ω_0 have a large contribution to the intensity interference. This manifests itself in an insufficiently truncated oscillation, as shown in Fig. 1(a). By increasing the power spectral density of high- and low-frequency components, the strong oscillation caused by the central components is suppressed more effectively. Furthermore, it is preferable for the spectrum to be asymmetric, with low frequency components being more intense, because then the spatial frequency of the oscillation decreases, and so does the demand for large Δk_x.

An example of an asymmetric super-Gaussian-type spectrum with a bandwidth of 20 nm is shown in Fig. 7(a). The light sheet generated with the designed compound prism is calculated using Eq. (10), yielding the intensity distribution shown in Fig. 7(b). In comparison with the light sheet of Fig. 5, the distribution has only one intensity peak, as can clearly be seen also in the transverse intensity distribution in Fig. 7(c). The intensity peak is narrower and the light sheet has a slightly shorter $z_{\max}$ (see Fig. 7(d)) that is still 5000 times longer than the peak width.

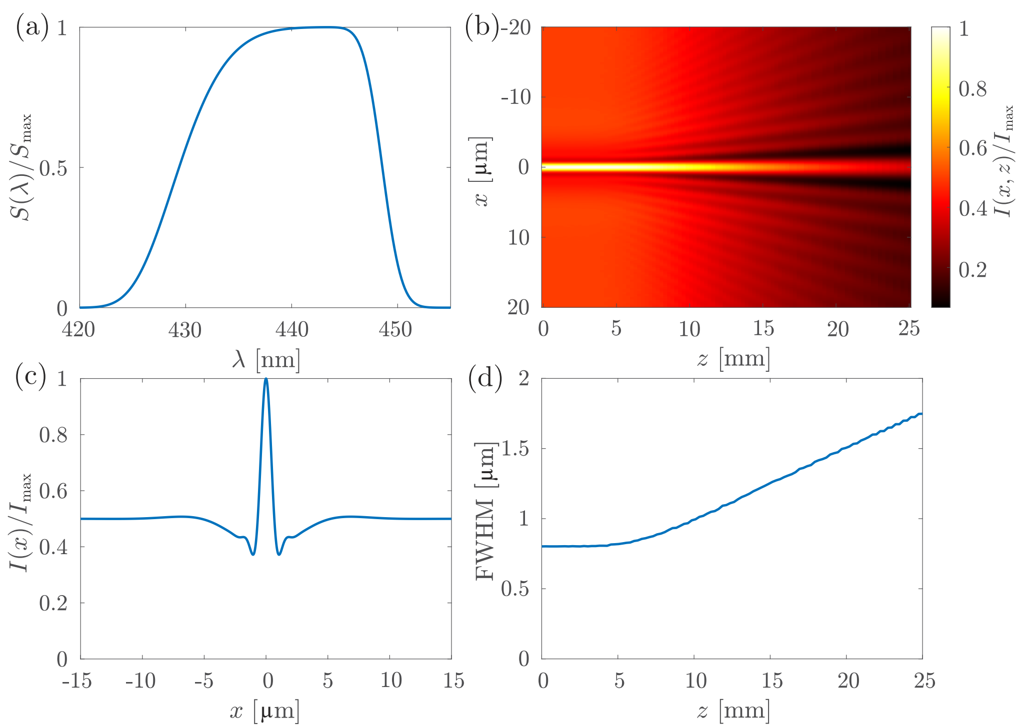

Fig. 7. Properties of a light sheet with an asymmetric super-Gaussian spectrum generated by using the designed compound prism: (a) the spectral power density; (b) the intensity distribution in the xz-plane; (c) the transverse intensity profile along the x-axis at $z = 1$ μm; (d) the FWHM of the light sheet as a function of propagation distance z.

In a dark sheet, insufficient truncation yields a strong intensity oscillation around the central minimum, as shown in Fig. 6. An asymmetric super-Gaussian spectrum of Fig. 7(a) can effectively eliminate the oscillation, as shown by the calculated intensity distributions along the transverse direction and in the xz-plane in Figs. 8(a) and (b), respectively.

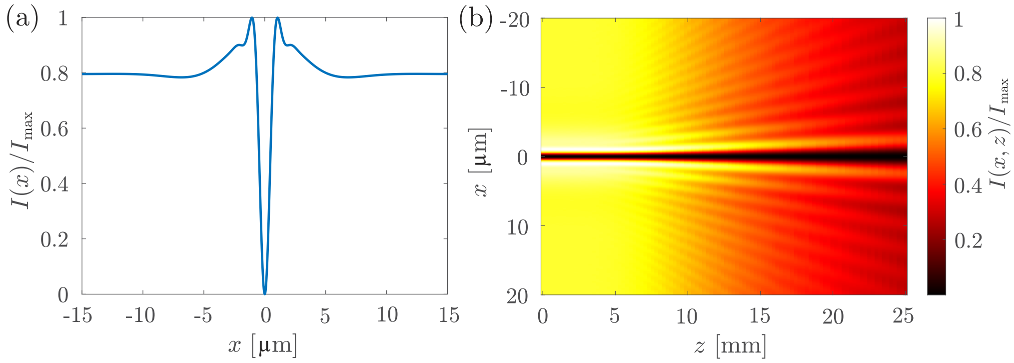

Fig. 8. Properties of a dark sheet with the asymmetric super-Gaussian spectrum of Fig. 7(a) generated by using the designed compound prism: (a) the transverse intensity profile along the x-axis at $z = 1$ μm; (b) the intensity distribution in the xz-plane.

5. Conclusion

We have introduced a prism-based approach for generating non-diffractive cw light sheets. Examples of generated bright and dark light sheets were modeled numerically, showing small sidelobes, exceptional thinness, and long diffraction-free propagation distance. These results are in agreement with the analytical model that we have derived for the light sheet intensity distribution. We have also shown that the light sheet could be refined by modifying its spectrum. We believe that the presented approach and the calculation results comprise a notable contribution to the technology of light sheet generation. Potential applications of the proposed light sheets range from optical trapping of particles with both positive and negative polarizabilities to three-dimensional imaging and light-sheet fluorescence microscopy. Compared to previously demonstrated light sheets, our sheets are cw and exceptionally long/extended at a given thickness. The price paid for that is a constant background intensity that is half of the on-axis intensity. For specific applications (e.g., in light-sheet microscopy), the background intensity can be reduced with a one-dimensional apodizing filter. This will shorten the low-divergence propagation distance in a controlled way, for example, to make it equal to the transverse size/extension of the observed field. In contrast, the dark sheets considered are completely dark and can be used, e.g., for stimulated-emission-depletion microscopy with high longitudinal resolution.

A. Derivation of Equation (8)

Inserting the spectral density $S(\omega) = E_0^2/\Delta\omega \exp[-2(\frac{\omega-\omega_0}{\Delta\omega})^2]$ and transverse wave numbers $k_x(\omega) = \omega/c[\sin\alpha_0 + \cos\alpha_0\partial_\omega\alpha_0(\omega-\omega_0)]$ into Eq. (1), we obtain

$$I(x) = \frac{E_0^2}{\Delta\omega}\int_0^\infty \exp\left[-2\left(\frac{\omega-\omega_0}{\Delta\omega}\right)^2\right]\cos^2\left\{\frac{\omega}{c}[\sin\alpha_0 + \cos\alpha_0\partial_\omega\alpha_0(\omega-\omega_0)]x - \frac{\varphi}{2}\right\}d\omega. \quad (17)$$

The squared cosine term can be expanded as $\cos^2(k_x x - \varphi/2) = 1/2(1 + \mathrm{Re}\{\exp(-i\varphi)\exp(2ik_x x)\}$, yielding

$$I(x) = \frac{E_0^2}{2\Delta\omega}\left(\int_{-\infty}^{\infty} \exp\left[-2\left(\frac{\omega-\omega_0}{\Delta\omega}\right)^2\right] d\omega \right.$$
$$\left. + \mathrm{Re}\left[\exp(-i\varphi)\int_0^{\infty} \exp\left\{-2\left(\frac{\omega-\omega_0}{\Delta\omega}\right)^2 + 2i\frac{\omega}{c}[\sin\alpha_0 + \cos\alpha_0\partial_\omega\alpha_0(\omega-\omega_0)]x\right\} d\omega\right]\right). \tag{18}$$

In Eq. (18), the lower integration limit of the first term has been extended to $-\infty$, resulting in a Gaussian integral

$$\int_{-\infty}^{\infty} \exp\left[-2\left(\frac{\omega-\omega_0}{\Delta\omega}\right)^2\right] d\omega = \Delta\omega\sqrt{\frac{\pi}{2}}. \tag{19}$$

The second integral can be expressed as

$$\begin{aligned} I_2 &= \int_0^{\infty} \exp\left\{-2\left(\frac{\omega-\omega_0}{\Delta\omega}\right)^2 + 2i\frac{\omega}{c}[\sin\alpha_0 + \cos\alpha_0\partial_\omega\alpha_0(\omega-\omega_0)]x\right\} d\omega \\ &= \Delta\omega\sqrt{\frac{\pi}{8}}\left\{1 + \mathrm{erf}\left[\frac{\sqrt{2}\omega_0}{\Delta\omega}\frac{1-iBx}{\sqrt{1-iAx}}\right]\right\}(1-iAx)^{-\frac{1}{2}} \\ &\times \exp\left[-\frac{\Delta\omega^2(\cos\alpha_0\partial_\omega\alpha_0\omega_0 + \sin\alpha_0)^2x^2}{2c^2[1+(Ax)^2]} + 2i\frac{\omega 0}{c}\sin\alpha_0 x\frac{1-ACx^2}{1+(Ax)^2}\right], \end{aligned} \tag{20}$$

where the parameters A, B, and C, are

$$A = \frac{\Delta\omega^2\cos\alpha_0\partial_\omega\alpha_0}{c}, \tag{21}$$

$$B = \frac{\Delta\omega^2(\cos\alpha_0\partial_\omega\alpha_0\omega_0 - \sin\alpha_0)}{2c\omega_0}, \tag{22}$$

$$C = \frac{\Delta\omega^2(\cos\alpha_0\partial_\omega\alpha_0\omega_0 - \sin\alpha_0)^2}{4c\omega_0\sin\alpha_0}. \tag{23}$$

Close to the axis of the light sheet, we have

$$|x| \ll \min\left\{\left|A^{-1}\right|, \left|B^{-1}\right|, \left|C^{-1}\right|\right\}, \tag{24}$$

which allows us to write the following approximate expression

$$I_2 = \Delta\omega\sqrt{\frac{\pi}{8}}\left\{1 + \mathrm{erf}\left[\frac{\sqrt{2}\omega_0}{\Delta\omega}\right]\right\}\exp\left[-\frac{\Delta\omega^2(\cos\alpha_0\partial_\omega\alpha_0\omega_0 + \sin\alpha_0)^2x^2}{2c^2} + 2i\frac{\omega_0}{c}\sin\alpha_0 x\right]. \tag{25}$$

Since $\sqrt{2}\omega_0/\Delta\omega \gg 1$, we have $\mathrm{erf}[\sqrt{2}\omega_0/\Delta\omega] \approx 1$. Noting also that $\omega_0/c\sin\alpha_0 = k_x(\omega_0)$ and

$$\partial_\omega k_x|_{\omega=\omega_0} = \frac{\cos\alpha_0\partial_\omega\alpha_0\omega_0 + \sin\alpha_0}{c} \approx \frac{\Delta k_x}{\Delta\omega}, \tag{26}$$

we simplify Eq. (25) and insert it together with Eq. (19) into Eq. (18), which eventually yields

$$I(x) = E_0^2\sqrt{\frac{\pi}{8}}\left\{1 + \exp\left[-\frac{1}{2}(\Delta k_x x)^2\right]\cos[2k_x(\omega_0)x - \varphi]\right\}. \tag{27}$$

Funding. Jenny ja Antti Wihurin Rahasto (00210075); Academy of Finland (308394); Aalto Science Institute AScI; Academy of Finland Flagship Programme, Photonics Research and Innovation (PREIN).

Optics EXPRESS

Disclosures. The authors declare no conflicts of interest.

Data availability. Data underlying the results presented in this paper are not publicly available at this time but may be obtained from the authors upon reasonable request.

References

1. H. T. Eyyuboğlu and Y. Baykal, "Analysis of reciprocity of cos-Gaussian and cosh-Gaussian laser beams in a turbulent atmosphere," Opt. Express **12**(20), 4659–4674 (2004).
2. C. Ding, L. Liao, H. Wang, Y. Zhang, and L. Pan, "Effect of oceanic turbulence on the propagation of cosine-Gaussian-correlated Schell-model beams," J. Opt. **17**(3), 035615 (2015).
3. F. G. Mitri, "Circularly-polarized Airy light-sheet spinner tweezers and particle transport," J. Quant. Spectrosc. Radiat. Transfer **260**, 107466 (2021).
4. F. G. Mitri, "Unconventional circularly polarized Airy light-sheet spinner tweezers," J. Opt. Soc. Am. A **38**(4), 526–533 (2021).
5. L. Li, T. Li, S. M. Wang, C. Zhang, and S. N. Zhu, "Plasmonic Airy Beam Generated by In-Plane Diffraction," Phys. Rev. Lett. **107**(12), 126804 (2011).
6. J. Lin, J. Dellinger, P. Genevet, B. Cluzel, F. de Fornel, and F. Capasso, "Cosine-Gauss Plasmon Beam: A Localized Long-Range Nondiffracting Surface Wave," Phys. Rev. Lett. **109**(9), 093904 (2012).
7. W. Müller, M. Kielhorn, M. Schmitt, J. Popp, and R. Heintzmann, "Light sheet Raman micro-spectroscopy," Optica **3**(4), 452–457 (2016).
8. A. P. Singh, J. W. Krieger, J. Buchholz, E. Charbon, J. Langowski, and T. Wohland, "The performance of 2D array detectors for light sheet based fluorescence correlation spectroscopy," Opt. Express **21**(7), 8652–8668 (2013).
9. P. A. Santi, "Light Sheet Fluorescence Microscopy: A Review," J. Histochem. Cytochem. **59**(2), 129–138 (2011).
10. O. E. Olarte, J. Andilla, E. J. Gualda, and P. Loza-Alvarez, "Light-sheet microscopy: A tutorial," Adv. Opt. Photonics **10**(1), 111–179 (2018).
11. J. M. Girkin and M. T. Carvalho, "The light-sheet microscopy revolution," J. Opt. **20**(5), 053002 (2018).
12. D. McGloin and K. Dholakia, "Bessel beams: Diffraction in a new light," Contemp. Phys. **46**(1), 15–28 (2005).
13. P. Hildén, E. Ilina, M. Kaivola, and A. Shevchenko, "Multifrequency Bessel beams with adjustable group velocity and longitudinal acceleration in free space," New J. Phys. **24**(3), 033042 (2022).
14. G. A. Siviloglou and D. N. Christodoulides, "Accelerating finite energy Airy beams," Opt. Lett. **32**(8), 979–981 (2007).
15. G. A. Siviloglou, J. Broky, A. Dogariu, and D. N. Christodoulides, "Observation of Accelerating Airy Beams," Phys. Rev. Lett. **99**(21), 213901 (2007).
16. A. Bencheikh, A. Bencheikh, S. Chabou, O. C. Boumeddine, H. Bekkis, A. Benstiti, L. Beddiaf, and W. Moussaoui, "Cosine beam: Diffraction-free propagation and self-healing," J. Opt. Soc. Am. A **37**(11), C7–C14 (2020).
17. Z. Jiang, "Truncation of a two-dimensional nondiffracting cos beam," J. Opt. Soc. Am. A **14**(7), 1478–1481 (1997).
18. C. J. R. Sheppard, "Pupil filters for generation of light sheets," Opt. Express **21**(5), 6339–6345 (2013).
19. D. Wilding, P. Pozzi, O. Soloviev, G. Vdovin, C. J. Sheppard, and M. Verhaegen, "Pupil filters for extending the field-of-view in light-sheet microscopy," Opt. Lett. **41**(6), 1205–1208 (2016).
20. I. Golub, B. Chebbi, and J. Golub, "Toward the optical "magic carpet": Reducing the divergence of a light sheet below the diffraction limit," Opt. Lett. **40**(21), 5121–5124 (2015).
21. M. Haouas, B. Chebbi, and I. Golub, "Extension of the span and optimization of the optical "magic carpet": Generation of a wide quasi-nondiffracting light sheet," J. Opt. Soc. Am. A **36**(1), 124–131 (2019).
22. M. Yessenov, L. A. Hall, K. L. Schepler, and A. F. Abouraddy, "Space-time wave packets," arXiv:2201.08297 (2022).
23. M. Yessenov, B. Bhaduri, H. E. Kondakci, M. Meem, R. Menon, and A. F. Abouraddy, "Non-diffracting broadband incoherent space-time fields," Optica **6**(5), 598–607 (2019).
24. B.-J. Chang, M. Kittisopikul, K. M. Dean, P. Roudot, E. S. Welf, and R. Fiolka, "Universal light-sheet generation with field synthesis," Nat. Methods **16**(3), 235–238 (2019).
25. B.-J. Chang and R. Fiolka, "Light-sheet engineering using the Field Synthesis theorem," JPhys Photonics **2**(1), 014001 (2020).
26. J. Tang and K. Y. Han, "Instantaneous non-diffracting light-sheet generation by controlling spatial coherence," Opt. Commun. **474**, 126154 (2020).
27. V. Ebrahimi, V. Ebrahimi, J. Tang, J. Tang, and K. Y. Han, "Incoherent superposition of polychromatic light enables single-shot nondiffracting light-sheet microscopy," Opt. Express **29**(20), 32691–32699 (2021).
28. J. W. Goodman, *Introduction to Fourier Optics* (Roberts & Co., 2005).
29. A. Shevchenko and T. Setälä, "Interference and polarization beating of independent arbitrarily polarized polychromatic optical waves," Phys. Rev. A **100**(2), 023842 (2019).
30. A. Shevchenko, M. Roussey, A. T. Friberg, and T. Setälä, "Ultrashort coherence times in partially polarized stationary optical beams measured by two-photon absorption," Opt. Express **23**(24), 31274–31285 (2015).
31. N. Hagen and T. S. Tkaczyk, "Compound prism design principles, I," Appl. Opt. **50**(25), 4998–5011 (2011).
32. H. E. Kondakci and A. F. Abouraddy, "Diffraction-free space–time light sheets," Nat. Photonics **11**(11), 733–740 (2017).

Optics EXPRESS

33. H. E. Kondakci, M. Yessenov, M. Meem, D. Reyes, D. Thul, S. R. Fairchild, M. Richardson, R. Menon, and A. F. Abouraddy, "Synthesizing broadband propagation-invariant space-time wave packets using transmissive phase plates," Opt. Express **26**(10), 13628–13638 (2018).
34. H. E. Kondakci and A. F. Abouraddy, "Optical space-time wave packets having arbitrary group velocities in free space," Nat. Commun. **10**(1), 929 (2019).
35. S. Basu, "Angular dispersion amplification method and apparatus for optical demultiplexing," *U.S. Patent* 7, 139, 447 (21 November 2006).
36. S. Basu, "Amplified dispersive delay generator using angular dispersion amplification," Appl. Opt. **48**(29), 5509–5513 (2009).
37. M. Debenham, "Refractive indices of zinc sulfide in the 0.405–13-*M*m wavelength range," Appl. Opt. **23**(14), 2238–2239 (1984).
38. "LASF35," Tech. rep., SCHOTT Advanced Optics US.